Multisensor Adaptive Bayesian Tracking under Time-Varying Target Detection Probability

Giuseppe Papa, *Student Member, IEEE,* Paolo Braca, *Member, IEEE,* Steven Horn, Stefano Marano, *Member, IEEE,* Vincenzo Matta, *Member, IEEE,* and Peter Willett, *Fellow, IEEE*

***Abstract*—In practical tracking applications the target detection performance may be unknown and also change rapidly in time. This work considers a network of sensors and develops a target tracking procedure able to adapt and react to the time-varying changes of the network detection probability. The proposed adaptive tracker is validated using extensive computer simulations and real-world experiments, testing a network of HF radars for maritime surveillance and an underwater network of AUVs for anti-submarine warfare.**

***Index Terms*—Adaptive target tracking, time-varying detection probability, data fusion, real-world experiment, HF surface wave radars, antisubmarine warfare, multistatic active sonar, underwater WSNs, AUV network, particle filtering.**

I. Introduction

TARGET tracking is a challenging problem which involves the joint detection and estimation of a time-varying and unknown number of targets based on the data of several sensors [2]. Measurements are usually subjected to noise, missed detections and false alarms. Such non-idealities of the collected returns are described in a statistical fashion, and the majority of target tracking algorithms assume some of the parameters that describe this statistical behaviour to be known.

However, in real applications these parameters may rapidly vary in time, largely due to propagation effects, medium nonstationarity, target aspect and similar issues, as discussed shortly. To some extent these are predictable from bathymetry, estimated target type and heading, etc., but such is unlikely to be perfect.

A typical scenario is that of maneuvering targets in which the behaviour of a target cannot be characterized at all times by a single dynamic model and a mechanism should estimate online the proper dynamics assumed by the target at the current time. This usual solution is often referred as an interacting multiple model (IMM) and assumes that a finite number of models can adequately describe the target behaviour in different regimes, see *e.g.* [22], [29], [46]. This approach has led to a considerable increase of the performance with respect to a tolerable increase of the computational cost [29].

In practical applications, a similar phenomenon can be observed for the performance of the sensors instead of the dynamics of the targets. Typically, in filtering problems the task of detecting – and sequestering – faulty sensors has been the one studied, see *e.g.* [3]; however, in target tracking problems, even if the sensor is working correctly, its capability of observing a target can be affected by several factors, often difficult to characterize and model properly. Consider the case in which the target aspect is not favorable in terms of geometry with respect to the sensor, or the signal-to-noise ratio (SNR) is completely unknown [13], degrading in both the cases the detection probability of the sensor. Another case is the interference in backscattered power due to the Bragg effect in high frequency surface wave (HFSW) radars [28]. In underwater sonar systems, target detections are influenced by several environmental effects – for instance sound propagation – which have a strong dependence on unknown parameters (*e.g.*, temperature, salinity, etc.) [11] that may change rapidly in time [4].

While a broad part of the target tracking literature considers the sensor performance as given, *e.g.*, see [5], [6], [8]–[10], [14], [15], [23], [25], [32], [44], and consequently the algorithm parameters perfectly matched, only few recent papers focus on the problem of a mismatch of the tracker parameters. In [35] a method is presented for determining the measurement noise covariance of a sensor, assumed to be constant, by using multiple IMM estimators while tracking targets of opportunity.

In [20] a Bayesian estimation method is proposed to sequentially update the probability of detection for tracking, in which a beta distribution is used for the prior. Then the Probabilistic Data Association (PDA) filter is used with the estimated detection probability but without considering track management. In [4] the authors study track management (confirmation and termination) routines for a multisensor sonar network where target detections are based on an underlying hidden Markov model (HMM) with high and low detection probability states. In [18] an augmented track state is proposed with an amplitude offset to predict the probability of detection for a target moving through a multistatic field. However, the results reported that the method was not effective in a multistatic field and was not able to predict probability of detection. In [13] the SNR is assumed to be unknown, and instead of trying to estimate the SNR of the target, an alternative approach is adopted, where the SNR is marginalized over a range of possible values, which results in an analytic solution for Rayleigh target likelihoods However, this approach is based on the assumption that the amplitudes of the measurements from true targets are stronger than those from clutter, which is a limitation in the most challenging cases of low-observable targets. In [27], [45],

G. Papa, P. Braca, S. Horn are with NATO STO Centre for Maritime Research and Experimentation, La Spezia, Italy, Email: {giuseppe.papa/paolo.braca/steven.horn}@cmre.nato.int.

S. Marano and V. Matta are with University of Salerno, Fisciano, Italy, Email: {marano/vmatta}@unisa.it.

P. Willett is with University of Connecticut, Storrs CT, Email: willett@engr.uconn.edu. P. Willett was supported by the U.S. Office of Naval Research under contract N000014-13-1-0231

the authors develop versions of the probability hypothesis density (PHD), cardinalized PHD (CPHD) and multi-Bernoulli filters that can adaptively learn both the clutter rate and detection profile while filtering, provided that such quantities do not change too rapidly compared to the measurement-update rate. In the proposed work instead we focus on the abrupt (time-varying) changes in the detection probability profile. Furthermore, the aforementioned procedures [27], [45] may require a high detection probability (as the case of the high SNR assumption in [13]), indeed in the simulation examples reported in [27], [45] the detection probability is always higher than 0.9, which is an unrealistic assumption in several radar/sonar applications where the targets can be low-observable. In [39] an extension of the standard PHD and CPHD filters is proposed that adaptively estimates the target birth intensity at each scan using the received measurements. In [19], [36], the authors propose a Bayesian inference approach to exploit target detections from multiple Automatic Identification System (AIS) sensors for the estimation of sensor performance and the number of targets. However, the AIS case is simplified by the absence of clutter measurements. In [21] a test statistic, which does not require prior knowledge of the detection probability, is proposed to support automatic track confirmation and termination decisions in a multiple hypotheses tracker (MHT).

The key aspect of the proposed work that is different from the aforementioned literature (e.g., [27], [45]) is that the sensor detection probability of a target is not only unknown and spatially dependent, but that it may change in time. Here the problem is tackled in the case of a sensor network, with different performance for each sensor – typically the single-sensor assumption is made.

A. Main results

A new target tracking procedure, referred as the *adaptive tracker*, is developed which is able to adapt to the changes of the sensor detection probability. In particular, a full Bayesian framework is derived to model the behaviour of a network of sensors in which each sensor has its own time-varying detection probability. The dynamic target state is then augmented with the detection probabilities of each sensor in the network (see also the discussion in [27], [45]). The dynamics of the detection probability are modeled as a time-varying Markov process. Two adaptive tracker approaches are developed in which i) the detection probability support is continuous and ii) the support is discrete. While in theory the discrete level case is expected to exhibit lower performance than the continuous level case, in several examples they perform equivalently. The only problem related to the discrete level approach is a possible mismatch of the selected discrete values with respect to the true ones. However, the most appealing advantage is that it requires low computational effort.

The proposed method is validated using extensive computer experiments, in which the comparison is done against the non-adaptive Bayesian filter and the clairvoyant filter which knows exactly the time-varying profile of the detection probability of the sensors.

The performance is evaluated in terms of mean optimal subpattern assignment (MOSPA) [41], [42], which is a metric for target tracking algorithms widely used and accepted in the literature. The proposed method exhibits performance often close to that of the clairvoyant system, and exhibits a significant improvement with respect to the non-adaptive filter.

The validation of the approach is achieved using two real-world experiments conducted by the NATO Science and Technology Organization - Centre for Maritime Research and Experimentation (CMRE). The approach is studied using a dataset collected during the CMRE HF-radar experiment, which took place between May and December 2009 on the Ligurian coast of the Mediterranean Sea (see more details in [28]). Also studied is a dataset collected during Proud Manta 2012 (ExPOMA12) using the CMRE underwater tracking system, composed of an underwater wireless sensor network (WSN) of autonomous underwater vehicles (AUVs) for anti-submarine warfare application (see also [11]).

In this paper the problem is most clearly formulated in terms of a single target. We feel, and we hope the reader agrees, that the concerns introduced by a need to track multiple targets are largely orthogonal to the challenges that we address here: time-varying and unknown probability of detection. The case of multiple well-separated targets can be tackled by classic multi-target tracking approaches[1]

The work presented in this paper is an extension of previously reported progress on the topic [37].

The remainder of this paper is organized as follows: the problem is formalized in Section II; the measurements model is described in Section III; the adaptive tracker is described in Section IV; the effectiveness of the proposed scheme, using synthetic data, is reported in Section V; results using real-world data are reported in Section VI; and conclusive remarks are provided in Section VII.

II. Problem Formalization

Consider a system consisting of a network of N sensors, whose aim is to monitor a surveillance region. In particular, the goal is to detect a target's presence or absence and, in the case of presence, to track the target state.

Without loss of generality, consider a two-dimensional surveillance region with area V. Similar to the formulation proposed for the Integrated Probabilistic Data Association (IPDA) [34], at time scan k one of the following hypotheses holds:

- $\mathcal{Q}$: the target is *absent*;
- $\mathcal{K}$: the target is *present*.

Also defined is $\mathcal{H}_k \in \{\mathcal{Q}, \mathcal{K}\}$ as the target present state at time scan k. Under $\mathcal{K}$, the target state is denoted by $\boldsymbol{x}_k = \left[x_k^1, \dot{x}_k^1, x_k^2, \dot{x}_k^2\right]^T$, where x_k^1 and x_k^2 are the positional coordinates (in keeping with our maritime application we are motivated by two-dimensional position) and $\dot{x}_k^1$ and $\dot{x}_k^2$ are the

[1] We mention a generalization of this method to the case of several sensors and several targets (not necessarily well-separated) that uses a belief propagation (BP) approach [30].

velocities in the two dimensions. The following set is defined for ease of notation:

$$X_k = \begin{cases} \emptyset, & \text{if } \mathcal{H}_k = \mathcal{Q}, \\ \{\boldsymbol{x}_k\}, & \text{if } \mathcal{H}_k = \mathcal{K}, \end{cases} \tag{1}$$

which is a compact representation of the target presence/absence and the target state. This formalization is strictly related to the (J)IPDA [33], [34], and its connection with the Random Finite Set (RFS) formulation is investigated in [12]. In the tracking literature, see *e.g.* [40], X_k is often referred to as a Bernoulli RFS with a probability density given by

$$\phi(X) = \begin{cases} 1-p, & \text{if } X = \emptyset, \\ p\ f(\boldsymbol{x}), & \text{if } X = \{\boldsymbol{x}\}, \end{cases} \tag{2}$$

where p is the probability of the target presence and $f(\boldsymbol{x})$ is the probability density function (PDF) of the target state. The time evolution of X_k is ruled by the probability density $\phi_X(X_k|X_{k-1})$ defined as

$$\phi_X(X_k|X_{k-1}) = \begin{cases} 1-p_b, & X_k = \emptyset, X_{k-1} = \emptyset, \\ p_b\ f_b(\boldsymbol{x}_k), & X_k = \{\boldsymbol{x}_k\}, X_{k-1} = \emptyset, \\ 1-p_s, & X_k = \emptyset, X_{k-1} = \{\boldsymbol{x}_{k-1}\}, \\ p_s\ f(\boldsymbol{x}_k|\boldsymbol{x}_{k-1}), & X_k = \{\boldsymbol{x}_k\}, X_{k-1} = \{\boldsymbol{x}_{k-1}\}, \end{cases} \tag{3}$$

where p_b and $f_b(\boldsymbol{x})$ are respectively the target *birth* probability and the target birth PDF, while p_s and $f(\boldsymbol{x}_k|\boldsymbol{x}_{k-1})$ are respectively the target *survival* probability and the target state transition PDF.

The target state transition distribution is often given by the relation

$$\boldsymbol{x}_k = f_k(\boldsymbol{x}_{k-1}, \boldsymbol{v}_k), \tag{4}$$

where f_k is the state transition function (generally non-linear) and $\boldsymbol{v}_k$ is the process noise, often assumed as a sequence of independent and identically distributed (i.i.d.) random variables.

A common formulation for (4) is the near constant velocity model (NCV)

$$\boldsymbol{x}_k = \boldsymbol{F}\boldsymbol{x}_{k-1} + \boldsymbol{A}\boldsymbol{v}_k, \tag{5}$$

where

$$\boldsymbol{F} = \begin{bmatrix} 1 & T & 0 & 0 \\ 0 & 1 & 0 & 0 \\ 0 & 0 & 1 & T \\ 0 & 0 & 0 & 1 \end{bmatrix}, \quad \boldsymbol{A} = \begin{bmatrix} T^2/2 & 0 \\ T & 0 \\ 0 & T^2/2 \\ 0 & T \end{bmatrix}, \tag{6}$$

T is the time between two consecutive scans and $\boldsymbol{v}_k$ is the two-dimensional acceleration noise vector modeled as an i.i.d. random process with Gaussian PDF $\mathcal{N}(\boldsymbol{v}; \boldsymbol{0}, \sigma_v^2 \boldsymbol{I}_2)$, which implies $f(\boldsymbol{x}_k|\boldsymbol{x}_{k-1}) = \mathcal{N}(\boldsymbol{x}_k; \boldsymbol{F}\boldsymbol{x}_{k-1}, \sigma_v^2 \boldsymbol{A}\boldsymbol{A}^T)$.

III. Measurement Model

This section describes the measurement origin uncertainty (MOU) model, widely used in the tracking literature to describe an observations process that allows for both missed detections and clutter [2].

At time scan k a sensor $s = 1, 2, \ldots, N$ can detect the target with a probability of detection, denoted by p_k^s. This probability is modeled in the proposed approach as time dependent. Furthermore, clutter measurements (not originated and independent from the target) are also observed. The set of the m_k^s measurements from sensor s at time scan k is denoted by

$$Z_k^s = \left\{\boldsymbol{z}_{k,i}^s, i = 1, 2, \ldots, m_k^s\right\}, \tag{7}$$

where $\boldsymbol{z}_{k,i}^s$ can be for instance a vector comprising range and bearing. If the target is present at time scan k, then the target originated measurement of the sensor s is given by

$$\boldsymbol{\theta}_k^s = \boldsymbol{h}_s(\boldsymbol{x}_k, \boldsymbol{w}_k^s), \tag{8}$$

where $\boldsymbol{h}_s$ is the measurement function and $\boldsymbol{w}_k^s$ is an i.i.d. measurement noise sequence. The target if detected generates at most one measurement for a given sensor s. If the target is detected then $\boldsymbol{\theta}_k^s \in Z_k^s$.

Since the sensors are conditionally independent given the target state, the likelihood of the measurements is [5]

$$\mathcal{P}(Z_k|X_k, \boldsymbol{p}_k) = \prod_{s=1}^{N} \mathcal{P}(Z_k^s|X_k, p_k^s), \tag{9}$$

where $Z_k \overset{def}{=} \{Z_k^1, \ldots, Z_k^N\}$ and $\boldsymbol{p}_k \overset{def}{=} \left[p_k^1, \ldots, p_k^N\right]^T$. The likelihood for the sensor s, under $\mathcal{Q}$ (target absent), is given only by clutter data

$$\mathcal{P}(Z_k^s|\emptyset, p_k^s) = \mathcal{P}(Z_k^s|\emptyset) = \phi_C^s(Z_k^s), \tag{10}$$

$$\phi_C^s(Z_k^s) = \begin{cases} m_k^s!\, \mu(m_k^s; \lambda^s) \prod\limits_{\boldsymbol{z} \in Z_k^s} c^s(z), & m_k^s > 0, \\ \mu(0; \lambda^s), & m_k^s = 0, \end{cases}$$

where $\mu(m; \lambda^s)$ and λ^s are respectively the distribution and the average number of clutter measurements, while $c^s(\boldsymbol{z})$ is the PDF of a clutter element. Often, $\mu(m; \lambda^s)$ is assumed to be Poisson and $c^s(z)$ to be uniform [5], [11]. It is worthwhile to mention that this approach does not model non-random clutter, which can be persistent and systematic, such as ground clutter in radar or shipwrecks in active sonar. Persistent clutter needs to be taken into account before the tracking stage.

Given $\mathcal{K}$, if $m_k^s > 0$, each of the following *association events* are possible within Z_k^s:

$$\begin{aligned} &\mathcal{A}_{0,s} : \boldsymbol{\theta}_k^s \notin Z_k^s, \\ &\mathcal{A}_{i,s} : \boldsymbol{z}_{k,i}^s = \boldsymbol{\theta}_k^s \in Z_k^s, \quad i = 1, \ldots, m_k^s \end{aligned} \tag{11}$$

and the likelihood related to sensor s can be rewritten as

$$\mathcal{P}(Z_k^s|\boldsymbol{x}_k, p_k^s) = \sum_{i=0}^{m_k^s} \mathcal{P}(Z_k^s|\boldsymbol{x}_k, p_k^s, \mathcal{A}_{i,s})\, \mathcal{P}\{\mathcal{A}_{i,s}|p_k^s\}, \tag{12}$$

where

$$\mathcal{P}(Z_k^s|\boldsymbol{x}_k, p_k^s, \mathcal{A}_{0,s}) = m_k^s!\, \mu(m_k^s; \lambda^s) \prod_{z \in Z_k^s} c^s(z), \tag{13}$$

$$\mathcal{P}(Z_k^s|\boldsymbol{x}_k, p_k^s, \mathcal{A}_{i,s}) = m_k^s!\, \mu(m_k^s - 1; \lambda^s)\, f\left(\boldsymbol{z}_{k,i}^s|\boldsymbol{x}_k\right) \prod_{z \in Z_k^s \setminus \boldsymbol{z}_{k,i}^s} c^s(z), \quad i = 1, \ldots, m_k^s \tag{14}$$

$$\mathcal{P}\{\mathcal{A}_{0,s}|p_k^s\} = 1 - p_k^s \tag{15}$$

$$\mathcal{P}\{\mathcal{A}_{i,s}|p_k^s\} = \frac{p_k^s}{m_k^s}, \quad i = 1, \ldots, m_k^s, \tag{16}$$

leading to

$$\mathcal{P}\left(Z_k^s|\boldsymbol{x}_k,p_k^s\right)=\left(1-p_k^s\right)\phi_C^s\left(Z_k^s\right)+ \\ +p_k^s\sum_{\boldsymbol{z}\in Z_k^s}f\left(\boldsymbol{z}|\boldsymbol{x}_k\right)\phi_C^s\left(Z_k^s\backslash\boldsymbol{z}\right). \quad (17)$$

In the case $m_k^s=0$ the likelihood becomes

$$\mathcal{P}\left(\emptyset|\boldsymbol{x}_k,p_k^s\right)=\phi_C^s\left(\emptyset\right)\left(1-p_k^s\right)=\mu\left(0;\lambda^s\right)\left(1-p_k^s\right). \quad (18)$$

It is worth noting that, for both cases $m_k^s>0$ and $m_k^s=0$, when $p_k^s=0$ (target not observable if present), the likelihoods (10) and (17) coincide and it is not possible to distinguish between the hypotheses $\mathcal{Q}$ and $\mathcal{K}$, see also the discussion in [33], [34]. In this work, the case of target not present and target not observable are both incorporated within the hypothesis $\mathcal{Q}$. Therefore, p_k^s is constrained such that it cannot have values below a given threshold $p_{min}^s>0$ under $\mathcal{K}$ to handle this ambiguity.

IV. Adaptive Tracker

In real-world applications, the performance of a sensor is usually time-varying because it depends on several factors, such as environmental conditions, interferences, etc. While in principle there could be the possibility to deterministically predict a degradation or increase of the sensor performance, often it is unclear if the accuracy of these predictions would be enough to guarantee that the target tracking algorithm can work optimally. The performance of a sensor is defined here as its ability to detect the target, quantified by the target detection probability introduced in the previous section. This quantity plays a fundamental role in a tracking procedure. For instance, consider having a single sensor and using the popular M/N logic where M detections (misses) out of N time scans are required to confirm (delete) a track (see details in [2], [28]). Let us select $M=2,N=3$ to confirm the track and $M=3,N=3$ to delete the track. Assume that the target is present and the true level of the initial detection probability is 90%. In this case, it would be very likely to correctly confirm a target track, in other words, to correctly detect the target presence. Now, if this probability were to decrease to a lower level, say 30%, then the track would be likely deleted prematurely. If it was known that the detection probability had decreased then one would choose different values of M and N.

In [4], assuming two possible levels for the detection probability, an adaptive track management logic is proposed that outperforms the non-adaptive procedure. In fact, it is shown that the track management performance achieved by ignoring the time variation of the detection probability – or even by accounting for it but ignoring its own inherent "trackability" – is orders of magnitude worse than could be achieved by accounting for it accurately. There is much room for improvement in such practical modeling, perhaps more than in any other aspect of target tracking.

In this work, it is noted that the likelihoods, defined in (10)-(17), strongly depend on the sensor detection probabilities. For this reason, a sequential Bayesian procedure is proposed, in which the detection probabilities are included in the dynamic system state. A similar approach can be adopted also in passive sonar applications, where the received signal power can be included in the system state. The state at time k is then redefined as $X_k=\{(\boldsymbol{x}_k,\boldsymbol{p}_k)\}$ when the target is present, while it remains $X_k=\emptyset$, when the target it absent. The posterior distribution given all the measurements up to time scan k is given by

$$\mathcal{P}\left(X_k|Z_{1:k}\right)=\frac{\mathcal{L}\left(Z_k|X_k\right)\mathcal{P}\left(X_k|Z_{1:k-1}\right)}{\mathcal{P}\left(Z_k|Z_{1:k-1}\right)}, \quad (19)$$

where $Z_{1:k}\overset{def}{=}\{Z_1,\ldots,Z_k\}$ and $\mathcal{L}\left(Z_k|X_k\right)$ is given by eqs. (9), (10) and (17), namely

$$\mathcal{L}\left(Z_k|\emptyset\right)=\prod_{s=1}^{N}\mathcal{P}\left(Z_k^s|\emptyset\right), \quad (20)$$

$$\mathcal{L}\left(Z_k|\left\{(\boldsymbol{x}_k,\boldsymbol{p}_k)\right\}\right)=\prod_{s=1}^{N}\mathcal{P}\left(Z_k^s|\boldsymbol{x}_k,\boldsymbol{p}_k\right). \quad (21)$$

The prediction term can be written as

$$\mathcal{P}\left(X_k|Z_{1:k-1}\right)=\mathbb{E}_X\left[\phi_X\left(X_k|X\right)|Z_{1:k-1}\right], \quad (22)$$

where $\mathbb{E}_X\left[a|b\right]$ is the conditional mean value of a given b, and the RFS transition density for the augmented state is indicated with $\phi_X\left(X_k|X_{k-1}\right)$. Note that this density has the same structure as eq. (3). There are two functions to be defined: the birth distribution $f_b\left(\boldsymbol{x}_k,\boldsymbol{p}_k\right)$, and the state transition distribution $f_{x,p}\left(\boldsymbol{x}_k,\boldsymbol{p}_k|\boldsymbol{x}_{k-1},\boldsymbol{p}_{k-1}\right)$.

Let us specify eq. (22) for the two hypotheses. The prediction term for $\mathcal{Q}$ is

$$\mathcal{P}\left(X_k=\emptyset|Z_{1:k-1}\right)=\left(1-p_b\right)\mathcal{P}\left(X_{k-1}=\emptyset|Z_{1:k-1}\right)+ \\ +\left(1-p_s\right)\left[1-\mathcal{P}\left(X_{k-1}=\emptyset|Z_{1:k-1}\right)\right]. \quad (23)$$

The prediction term for $\mathcal{K}$ is given by two contributes

$$\mathcal{P}\left(X_k=\left\{(\boldsymbol{x}_k,\boldsymbol{p}_k)\right\}|Z_{1:k-1}\right)=g_b\left(\boldsymbol{x}_k,\boldsymbol{p}_k\right)+g_p\left(\boldsymbol{x}_k,\boldsymbol{p}_k\right), \quad (24)$$

where

$$g_b\left(\boldsymbol{x}_k,\boldsymbol{p}_k\right)=p_b\,\mathcal{P}\left(X_{k-1}=\emptyset|Z_{1:k-1}\right)f_b\left(\boldsymbol{x}_k,\boldsymbol{p}_k\right) \quad (25)$$

$$g_p\left(\boldsymbol{x}_k,\boldsymbol{p}_k\right)=p_s\left[1-\mathcal{P}\left(X_{k-1}=\emptyset|Z_{1:k-1}\right)\right] \\ \times\mathbb{E}_{(\boldsymbol{x},\boldsymbol{p})}\left[f_{x,p}\left(\boldsymbol{x}_k,\boldsymbol{p}_k|\boldsymbol{x},\boldsymbol{p}\right)|Z_{1:k-1}\right] \quad (26)$$

Given that the target motion is independent of the detection probabilities, the state transition distribution $f_{x,p}\left(\boldsymbol{x}_k,\boldsymbol{p}_k|\boldsymbol{x}_{k-1},\boldsymbol{p}_{k-1}\right)$ can be factored as

$$f_{x,p}\left(\boldsymbol{x}_k,\boldsymbol{p}_k|\boldsymbol{x}_{k-1},\boldsymbol{p}_{k-1}\right)=f\left(\boldsymbol{x}_k|\boldsymbol{x}_{k-1}\right)f_p\left(\boldsymbol{p}_k|\boldsymbol{p}_{k-1},\boldsymbol{x}_k\right), \quad (27)$$

where $f_p\left(\boldsymbol{p}_k|\boldsymbol{p}_{k-1},\boldsymbol{x}_k\right)$ is the detection probability transition distribution, formally dependent on the target state (*e.g.*, the target-sensor geometry). Assuming that the sensors are conditionally independent, the detection probability transition distribution is given by

$$f_p(\boldsymbol{p}_k|\boldsymbol{p}_{k-1},\boldsymbol{x}_k)=\prod_{s=1}^{N}f_p^s(p_k^s|p_{k-1}^s,\boldsymbol{x}_k), \quad (28)$$

where each $f_p^s(p_k^s|p_{k-1}^s, \boldsymbol{x}_k)$ is the transition distribution of the corresponding p_k^s of the sensor s. It is worthwhile to remark that the dependency on the target state in (27)-(28) can model several physical behaviours. For instance, considering the Bragg effect in the HFSW radars (see details in [28]), when the target sails with a radial velocity within the Bragg region the radiation backscattered from the sea dominates the target return leading to a possible significant degradation of the performance. Another example is that of the dependency on target-sensor geometry, in which, for instance, when the target is broadside with respect to the sensor there is a significant improvement of the performance. Different models of the transition distribution for the detection probability are considered in the following subsections.

A. Continuous-valued Detection Probability

In this subsection we describe the detection probability transition distribution. This distribution is assumed to have a continuous support in the range $\Omega_s = [p_{min}^s, 1]$ and to be independent of the target state.

A first simple but effective approach to formalize the variation in time of the detection probability is that of using a linear model, but forcing the probability to remain in the range Ω_s. This model is popular in several contexts, for instance in the modeling of target dynamics. In the aforementioned NCV the variation in time of the velocity is modeled by a random acceleration. The value of p_k^s is a clamped version of the sum of its previous value plus a random quantity n_k^s:

$$p_k^s = \begin{cases} p_{min}^s, & p_{k-1}^s + n_k^s < p_{min}^s, \\ 1, & p_{k-1}^s + n_k^s > 1, \\ p_{k-1}^s + n_k^s, & \text{otherwise.} \end{cases} \tag{29}$$

Assuming $n_k^s \sim \mathcal{N}\left(n; 0, \sigma_s^2\right)$, $f_p\left(p_k^s|p_{k-1}^s\right)$ is a distribution of mixed type with two masses in p_{min}^s and 1 equal to $1 - Q\left(\frac{p_{min}^s - p_{k-1}^s}{\sigma_s}\right)$ and $Q\left(\frac{1-p_{k-1}^s}{\sigma_s}\right)$, respectively, where $Q(a) \stackrel{def}{=} \int_a^{+\infty} \mathcal{N}(x; 0, 1)dx$ is the standard normal exceedance probability. In the range $p_{min}^s < p_k^s < 1$, $f_p\left(p_k^s|p_{k-1}^s\right)$ is the normal distribution $\mathcal{N}\left(p_k^s; p_{k-1}^s, \sigma_s^2\right)$.

A different model employs the beta distribution [45]: $f_p\left(p_k^s|p_{k-1}^s\right)$ has a mass in p_{min}^s equal to $F_\beta(p_{min}^s; a_{k-1}, b_{k-1})$ and in the range $p_{min}^s < p_k^s \leq 1$ is the beta distribution $\beta\left(p_k^s; a_{k-1}, b_{k-1}\right)$, where we have defined $F_\beta(x; a, b) = \int_0^x \beta\left(t; a, b\right) dt$ as the cumulative distribution function of the beta random variable. As in [45], the parameters of the beta distribution are selected as $a_{k-1} = (p_{k-1}^s(1 - p_{k-1}^s)/\sigma_s^2 - 1)p_k^s$ and $b_{k-1} = (p_{k-1}^s(1 - p_{k-1}^s)/\sigma_s^2 - 1)(1 - p_k^s)$, so that, for $p_{min}^s \approx 0$, $E\left[p_k^s|p_{k-1}^s\right] \approx p_{k-1}^s$ and $\text{VAR}\left[p_k^s|p_{k-1}^s\right] \approx \sigma_s^2$.

This approach will be referred to as the *continuous-support adaptive tracker* (C-adaptive tracker).

B. Discrete-valued Detection Probability

In the previous section it was assumed that p_k^s takes values in the continuous range $[p_{min}^s, 1]$, $s = 1, \ldots, N$. Next, it is instead considered that p_k^s can only have values from the discrete set

$$\Omega_s = \left\{\omega_1^s, \ldots, \omega_{L_s}^s\right\}, \tag{30}$$

where $\omega_i^s \in [p_{min}^s, 1]$, $\forall i = 1, \ldots, L_s$. The state p_k^s then evolves according to a Markov Chain (MC) with a given transition matrix $\boldsymbol{P}^s \in [0, 1]^{L_s \times L_s}$, which satisfies the conditions

$$\sum_{j=1}^{L_s} \{\boldsymbol{P}^s\}_{i,j} = 1, \qquad \forall i = 1, \ldots, L_s, \tag{31}$$

where $\{\boldsymbol{P}^s\}_{i,j}$ indicates the element i, j of $\boldsymbol{P}^s$ and represents the transition probability

$$\{\boldsymbol{P}^s\}_{i,j} = f_p\left(p_k^s = \omega_j^s | p_{k-1}^s = \omega_i^s\right). \tag{32}$$

The elements in $\boldsymbol{P}^s$ are selected in order to tune the adaptivity of the tracker to the sensor performance changes. For instance, in the case of a more conservative setup, the elements on the diagonal will be prevalent on off-diagonal elements, while in the case of a more reactive setup, the probability is larger on off-diagonal elements.

This approach will be referred to as the *discrete-support adaptive tracker* (D-adaptive tracker).

C. Non-adaptive Tracker

The standard target tracking procedure assumes a given fixed probability of detection for all time scans, *i.e.*, $p_k^s = p^s, \forall k, s$. In this case, the posterior distribution can be computed particularizing the expression of the D-adaptive tracker with $L_s = 1$ and $\omega_1^s = p^s$, $\forall s$. This approach will be referred to as the *non-adaptive tracker*.

D. Inference Procedure

In this subsection we describe the estimation procedure for obtaining $\widehat{X}_k$ from the posterior distribution $\mathcal{P}\left(X_k|Z_{1:k}\right)$. As discussed in the literature, see *e.g.* [9], [26], [33], [34], in this work we opt for a two-stage procedure in which first we decide if the target is present or absent and then estimate its state. Given our Bayesian detection framework, the optimal decision rule is formulated as follows [38]

$$\begin{cases} \mathcal{P}\left(X_k \neq \emptyset | Z_{1:k}\right) \geq p_\gamma, & \text{declare } \widehat{\mathcal{H}}_k = \mathcal{K}, \\ \mathcal{P}\left(X_k = \emptyset | Z_{1:k}\right) > 1 - p_\gamma, & \text{declare } \widehat{\mathcal{H}}_k = \mathcal{Q}, \end{cases} \tag{33}$$

where p_γ is named as target probability threshold. The estimator is then given by

$$\widehat{X}_k = \begin{cases} \{(\widehat{\boldsymbol{x}}_k, \widehat{\boldsymbol{p}}_k)\}, & \text{if } \widehat{\mathcal{H}}_k = \mathcal{K}, \\ \emptyset, & \text{if } \widehat{\mathcal{H}}_k = \mathcal{Q}, \end{cases} \tag{34}$$

where $\widehat{\boldsymbol{x}}_k$ and $\widehat{\boldsymbol{p}}_k$ are the estimator of the target state and the detection probabilities. A convenient choice for the target state, optimal in terms of mean square error, is the posterior mean $\widehat{\boldsymbol{x}}_k = \mathbb{E}\left[\boldsymbol{x}_k|Z_{1:k}\right]$. Another suitable estimator is the posterior mode $\widehat{\boldsymbol{x}}_k = \arg\max_{\boldsymbol{x}_k} \mathcal{P}\left(\boldsymbol{x}_k|Z_{1:k}\right)$. Analogously, we can proceed for the profile of the detection probabilities $\widehat{\boldsymbol{p}}_k$.

Note that this estimation procedure is equivalent to the GMAP-I estimator proposed in [17] when $p_\gamma = 0.5$.

Algorithm 1 Adaptive Tracker using particle filtering.

IMPORTANCE SAMPLING

Propagation

Draw $\boldsymbol{x}_k^i \sim f\left(\boldsymbol{x}_k|\boldsymbol{x}_{k-1}^i\right)$, $\forall i = 1,\ldots,N_p$;

Draw $\boldsymbol{p}_k^i \sim f_p\left(\boldsymbol{p}_k|\boldsymbol{p}_{k-1}^i\right)$, $\forall i = 1,\ldots,N_p$;

New particles

Draw N_u new samples $\boldsymbol{x}_k^i$ from $\mathcal{U}(\boldsymbol{x})$ and $\boldsymbol{p}_k^i$ from $\mathcal{U}(\boldsymbol{p})$;

for $s = 1$ **to** N **do**

  Draw N_n new samples $\boldsymbol{x}_k^i$ from $\mathcal{U}\left(\boldsymbol{x};\boldsymbol{z}_{k,i}^s\right)$ and $\boldsymbol{p}_k^i$ from $\mathcal{U}(\boldsymbol{p})$, $\forall i = 1,\ldots,|Z_k^s|$;

end for

UPDATE

for $i = 1$ **to** $N_p + N_u + N_n N_{Z_k}$ **do**

  $X_k^i = \left\{\left(\boldsymbol{x}_k^i, \boldsymbol{p}_k^i\right)\right\}$, $w_k^i = \mathcal{L}\left(Z_k|X_k^i\right)\frac{\phi_X\left(X_k^i|X_{k-1}^i\right)}{q\left(X_k^i|X_{k-1}^i,Z_k\right)}w_{k-1}^i$;

end for

$w_k^\emptyset = \mathcal{L}\left(Z_k|X_k=\emptyset\right)\left[(1-p_b)\,w_{k-1}^\emptyset + (1-p_s)\left(1-w_{k-1}^\emptyset\right)\right]$;

Drop the particles with the lowest $N_u + N_n N_{Z_k}$ weights;

NORMALIZATION

$w_t = w_k^\emptyset + \sum_{j=1}^{N_p} w_k^i$; {Total weight}

$w_k^i = \frac{w_k^i}{w_t}$, $\forall i = 1,\ldots,N_p$;

$w_k^\emptyset = \frac{w_k^\emptyset}{w_t}$;

RESAMPLING

$N_{eff} = \left(\sum_{j=1}^{N_p} {w_k^i}^2\right)^{-1}$; {Effective sample size}

if $N_{eff} < N_p T_d$ **then**

  resampling;

end if

E. Particle Filter Implementation

Since the exact form of (19) is difficult (or even impossible) to derive, a numerical implementation of the tracker, based on the Sequential Monte Carlo methods [1], [43] is used. The posterior distribution at time scan k in (19) is represented by [43]

$$\hat{\mathcal{P}}\left(X_k|Z_{1:k}\right) = \begin{cases} w_k^\emptyset, & X_k = \emptyset, \\ \sum_{i=1}^{N_p} w_k^i \delta_{\boldsymbol{x}_k^i,\boldsymbol{p}_k^i}(\boldsymbol{x},\boldsymbol{p}), & X_k = \{(\boldsymbol{x},\boldsymbol{p})\}, \end{cases} \tag{35}$$

where $w_k^\emptyset$ is the weight approximating $\mathcal{P}\left(X_k=\emptyset|Z_{1:k}\right)$, while w_k^i is the weight of the i-th sample of the augmented system state $X_k^i = \left\{\left(\boldsymbol{x}_k^i,\boldsymbol{p}_k^i\right)\right\}$, approximating $\mathcal{P}\left(X_k^i|Z_{1:k}\right)$, and N_p is the number of particles. The initial samples $\boldsymbol{x}_0^i$ are uniformly drawn in the surveillance area for the positional coordinates and in $[-v_{max}, v_{max}]$ for the speed coordinates, while the initial samples $\boldsymbol{p}_0^i$ are uniformly drawn in $\Omega_1 \times \cdots \times \Omega_N$, and the corresponding weights w_0^i are all initialized to $(2N_p)^{-1}$, while $w_0^\emptyset = 0.5$. In the importance sampling step of the tracker, the augmented system state transition distribution is used to propagate the new samples $\left(\boldsymbol{x}_k^i,\boldsymbol{p}_k^i\right)$, $\forall i = 1,\ldots,N_p$, from the N_p samples at the previous step. New particles are generated as follows: $\forall i = N_p+1,\ldots,N_p+N_u$ particles are uniformly sampled on the augmented state space (as in the initialization); $\forall i = N_p+N_u+1,\ldots,N_p+N_u+N_n N_{Z_k}$, where $N_{Z_k} = \sum_{s=1}^{N}|Z_k^s|$, the measurements collected by all the sensors Z_k at step k are used to generate other particles. In particular, for each measurement $\boldsymbol{z} \in Z_k^s$, $\forall s = 1,\ldots,N$, N_n particles $\left(\boldsymbol{x}_k^i,\boldsymbol{p}_k^i\right)$ are sampled, where $\boldsymbol{x}_k^i$ is drawn from $\mathcal{U}(\boldsymbol{x};\boldsymbol{z})$, which is for the speed coordinates a uniform distribution in $[-v_{max}, v_{max}]$ and for the positional coordinates a uniform distribution, centered in $\boldsymbol{z}$, with a square support of area ν. The detection probability sample $\boldsymbol{p}_k^i$ is drawn from $\mathcal{U}(\boldsymbol{p})$, which is the uniform distribution in $\Omega_1 \times \cdots \times \Omega_N$.

Accordingly to the RFS particle filter implementation [43], the weight of $X_k^i = \left\{\left(\boldsymbol{x}_k^i,\boldsymbol{p}_k^i\right)\right\}$ is updated as follows

$$w_k^i = \mathcal{L}\left(Z_k|X_k^i\right)\frac{\phi_X\left(X_k^i|X_{k-1}^i\right)}{q\left(X_k^i|X_{k-1}^i,Z_k\right)}w_{k-1}^i, \tag{36}$$

where $\phi_X\left(X_k|X_{k-1}\right)$ is the augmented state transition density and $q\left(X_k|X_{k-1},Z_k\right)$ is the importance sampling density. In (36) the ratio of these latter densities is given by

$$\frac{\phi_X\left(X_k^i|X_{k-1}^i\right)}{q\left(X_k^i|X_{k-1}^i,Z_k\right)} = \begin{cases} p_s & i = 1,\ldots,N_p, \\ p_{b,k} & i = N_p+1,\ldots,N_p+N_u, \\ p_{b,k}\frac{\nu}{V} & i = N_p+N_u+1,\ldots,N_p+N_u+N_n N_{Z_k}, \end{cases} \tag{37}$$

where it was assumed a uniform birth density, and $p_{b,k} \stackrel{def}{=} \frac{p_b w_{k-1}^\emptyset}{N_u+N_n N_{Z_k}}$. In view of eq. (23), for $X_k = \emptyset$ the weight is updated as follows

$$w_k^\emptyset = \mathcal{L}\left(Z_k|\emptyset\right)\left[(1-p_b)\,w_{k-1}^\emptyset + (1-p_s)\left(1-w_{k-1}^\emptyset\right)\right]. \tag{38}$$

The $N_u + N_n N_{Z_k}$ particles with the lowest weight are dropped, and then the other N_p particles are normalized. The resampling step is standard and given in [1], [43].

The implementation, described above, is detailed in Algorithm 1.

Finally, applying the inference procedure reported in the previous subsection, the state estimator at time scan k is

$$\widehat{X}_k = \begin{cases} \{(\widehat{\boldsymbol{x}}_k,\widehat{\boldsymbol{p}}_k)\}, & \text{if } 1-w_k^\emptyset \geq p_\gamma, \\ \emptyset, & \text{if } w_k^\emptyset > 1-p_\gamma, \end{cases} \tag{39}$$

where the target state is estimated as

$$\widehat{\boldsymbol{x}}_k = \frac{\sum_{i=1}^{N_p}\boldsymbol{x}_k^i w_k^i}{1-w_k^\emptyset}, \tag{40}$$

and the detection probabilities are estimated as the mode of the approximated posterior distribution.

V. Computer Experimental Results

This section compares the effectiveness of the adaptive and non-adaptive trackers by using computer simulated data.

The sensors return position measurements in polar coordinates in all of the considered scenarios, namely range and bearing angle.

The clutter measurements from all sensors are assumed to be uniformly distributed in the surveillance area, namely $c^s(z) = 1/V$ (here z is expressed in Cartesian coordinates), while $\mu(m;\lambda^s)$ is assumed to be Poisson with average value

λ^s. The cases of both monostatic sensors (source and receiver are co-located) and bistatic sensors (source and receiver are in two different positions) are considered. If sensor s is monostatic then eq. (8) becomes

$$\boldsymbol{z}_k^s = \begin{bmatrix} \|\boldsymbol{d}_k - \boldsymbol{d}_{s,k}\| \\ \arctan\left(\frac{x_k^2 - d_{s,k}^2}{x_k^1 - d_{s,k}^1}\right) - h_{s,k} \end{bmatrix} + \boldsymbol{w}_k^s, \tag{41}$$

where $\boldsymbol{d}_k = \left[x_k^1, x_k^2\right]^T$ is the target position, $\boldsymbol{d}_{s,k} = \left[d_{s,k}^1, d_{s,k}^2\right]^T$ is the sensor position, and $h_{s,k}$ is the sensor heading. If sensor s is bistatic then eq. (8) becomes

$$\boldsymbol{z}_k^s = \begin{bmatrix} \|\boldsymbol{d}_k - \boldsymbol{p}_{s,k}\| + \|\boldsymbol{d}_k - \boldsymbol{t}_{s,k}\| \\ \arctan\left(\frac{x_k^2 - d_{s,k}^2}{x_k^1 - d_{s,k}^1}\right) - h_{s,k} \end{bmatrix} + \boldsymbol{w}_k^s, \tag{42}$$

where $\boldsymbol{t}_{s,k} = \left[t_{s,k}^1, t_{s,k}^2\right]^T$ is the source position. In both (41) and (42) $\boldsymbol{w}_k^s$ is the two-dimensional i.i.d. measurement noise process distributed according to $\mathcal{N}\left(\boldsymbol{0}, \begin{bmatrix} \sigma_r^{s\,2} & 0 \\ 0 & \sigma_b^{s\,2} \end{bmatrix}\right)$. Note that the measurements are converted in Cartesian coordinates, and the related PDF is computed using the random variable transformation theorem, as explained in [11].

A. Synthetic Scenario

Consider the scenario reported in Fig. 1, in which a target is sailing North-West. Synthetic data are generated by simulating two sensors for 90 time scans according to the MOU model, described in Section III. A bistatic geometry for the first sensor and a monostatic geometry for the second one is used. The overall contact history (blue dots for the first sensor and black dots for the second one) is reported in Fig. 1(a), along with the sensor and source positions and the true and estimated target trajectories.

The simulation can be divided into three intervals. In the first two intervals the target is present while in the last one the target disappears. In the first interval the detection probability is relatively large, 0.9 for both the sensors, while in the second part it abruptly decreases to 0.3 for both the sensors, see Fig. 1(b). The non-adaptive tracker is matched to the highest value of detection probability (first interval) for both sensors. The C-adaptive tracker is set up with $p_{min}^s = 0.2$ and $\sigma_s = 0.05$ for both sensors. The target presence threshold p_γ, defined in (33), is set to 0.8 for both the C-adaptive and non-adaptive trackers. The other common parameters are reported in Tab. I. Fig. 1(c) compares the simulated target path (ground-truth) to the tracks, generated by the non-adaptive and C-adaptive trackers, when the target is declared as present.

TABLE I
PARAMETER VALUES USED IN THE ALGORITHM FOR SIMULATED DATA.

Par.	*Value*	*Specification*
T	40 s	Time scan
σ_v	$5\ 10^{-3}$ m/s^2	Process noise
σ_r	75 m	Range standard deviation
σ_b	1°	Bearing standard deviation
λ/V	$1.2\,10^{-8}$ m^{-2}	Clutter density
N_p	$5\ 10^4$	Number of particles
p_b	10^{-2}	Birth probability
p_s	$1 - 10^{-3}$	Survival probability
N	2	Number of sensors
N_u	2500	Uniform particles per scan
N_n	250	Particles per measurement
T_d	0.5	Degeneracy threshold
ν	10^4	Area of birth particles

Fig. 1(d) shows the target presence (1 for target present and 0 for target absent) and the posterior target presence probability, namely $1 - \mathcal{P}\left(X_k = \emptyset | Z_{1:k}\right)$, for the considered trackers. It is evident that the C-adaptive tracker is able to track the target for a longer time with respect to the non-adaptive one. In particular the non-adaptive tracker detects the target until $k = 36$, while the C-adaptive is able to detect the target until its disappearance at $k = 60$ and correctly deletes the track after just 4 time scans. These different behaviors are apparently given by the role of the detection probability: after $k = 30$ the non-adaptive tracker continues to use the high value (0.9) of detection probability while the true value is 0.3, consequently it expects the target to be detected more often than it actually is and thus its posterior target probability decreases, misinterpreting the data and declaring the target absence; conversely, the C-adaptive tracker is able to recognize the change of the detection probability (cf. Fig. 1(b) where the mode of the posterior distribution of the detection probability is reported for both the sensors) and is able to track the target until the end.

When the target disappears, the absence of the target is equivalent to a null detection probability while the minimum value of the detection probability in the algorithm is 0.2. We observe that the estimated detection probability is quite noisy. We think that the lower the detection probability, the more difficult be the estimation of the detection probability: the case of no target is perhaps an extreme case in which the estimation is, well, quite poor. However, the most important task of the filter in this case is to avoid false alarms and to be ready in the case that the target appears again in the next scans. This task is well accomplished by the proposed procedure.

Figs. 1(e) and 1(f) report the estimation error in position and speed, respectively. Assuming that the target is always declared as present in the first two intervals (equivalent to the case where $p_\gamma = 0$), it can be noted that until $k = 36$ the two trackers present about the same error, while $\forall k = 37, \ldots, 60$ the error of the non-adaptive tracker is considerably higher than the C-adaptive tracker for both position and speed, which can be ascribed to the mismatch of the probability of detection.

B. Monte Carlo Simulations

In this subsection the performance of the adaptive and non-adaptive trackers are evaluated in terms of MOSPA [41], [42]. This metric takes into account the estimation error when the target is correctly detected as well as the missed detections, which are quantified by a parameter c. In this setup, the optimal subpattern assignment (OSPA) at time scan k is expressed as

$$\text{OSPA}_k = \begin{cases} \min\left(c, \|\hat{\boldsymbol{p}}_k - \boldsymbol{p}_k\|\right), & \text{decide } \mathcal{K} \text{ under } \mathcal{K}, \\ c, & \text{decide } \mathcal{Q} \text{ under } \mathcal{K}, \\ c, & \text{decide } \mathcal{K} \text{ under } \mathcal{Q}, \\ 0, & \text{decide } \mathcal{Q} \text{ under } \mathcal{Q}. \end{cases} \tag{43}$$

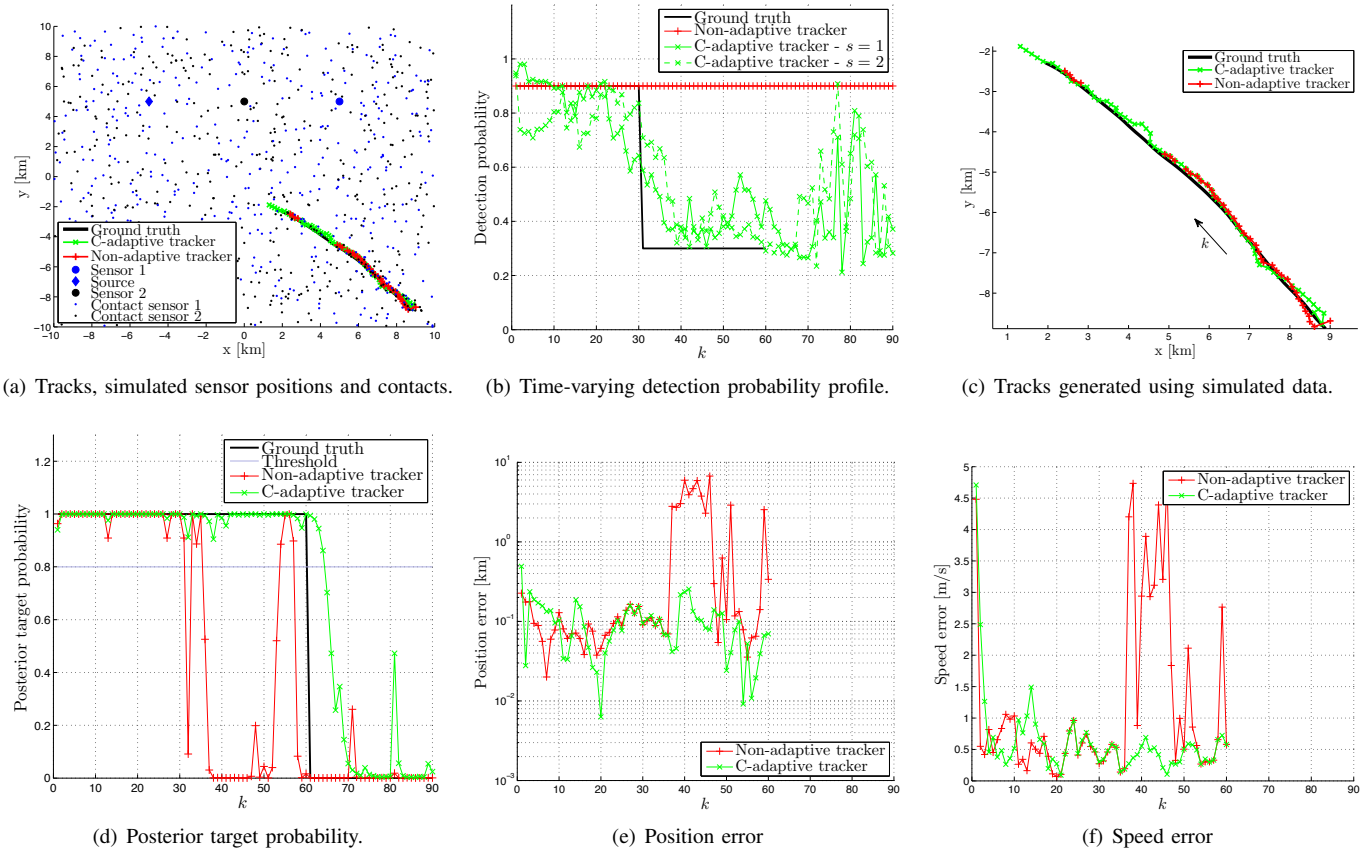

(a) Tracks, simulated sensor positions and contacts. (b) Time-varying detection probability profile. (c) Tracks generated using simulated data.

(d) Posterior target probability. (e) Position error (f) Speed error

Fig. 1. Comparison between the C-adaptive and non-adaptive tracker using simulated data. Panel (a) shows the simulated surveillance area with the target trajectories, the sensor and source positions and the simulated contacts. Panel (b) presents the value of the detection probability, constant and fixed to 0.9 for the non-adaptive tracker, while for the C-adaptive tracker we report the mode of the posterior distribution of the detection probability for the two sensors, $s = 1, 2$. An abrupt change in the true detection probability is simulated at the time scan $k = 30$. In panel (c) the trajectories when the target is declared as present are reported. Note that the track from the C-adaptive tracker is obscured by that of the non-adaptive one, but that it emerges after the latter's track is lost. Panel (d) shows the target presence (ground-truth) and the posterior target probability. The target disappears at time scan $k = 60$. Panel (e) and (f) report the error between the estimated track and the simulated data in position and speed, respectively.

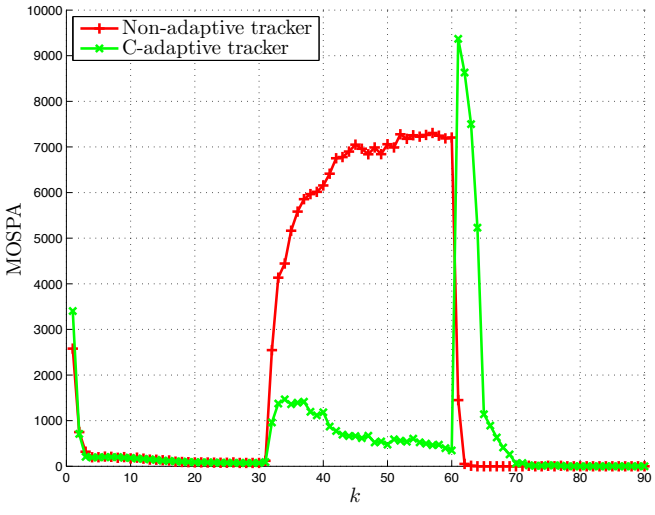

Fig. 2. Comparison between the C-adaptive and non-adaptive tracker in terms MOSPA using simulated data generated by the synthetic scenario described in Subsection V-A.

TABLE II
RELATIVE GAIN (PERCENT) IN MOSPA UNDER $\mathcal{K}$ OF THE ADAPTIVE TRACKERS WITH RESPECT TO THE NON-ADAPTIVE TRACKER.

A	MOSPA|$\mathcal{Q}$	91	165	272	454	677	1038
	C-adaptive	21.7	19.7	15.4	12.9	13.4	14.3
	D-adaptive	18.9	18.2	14.5	12	12	12.9
B	MOSPA|$\mathcal{Q}$	99	190	288	425	648	1061
	C-adaptive	26.7	21.3	20.1	20.4	21.2	21.8
	D-adaptive	23.9	18.1	16.9	16.9	17.5	18.2
C	MOSPA|$\mathcal{Q}$	96	170	244	312	510	1011
	C-adaptive	5.1	5	4.9	4.8	4.8	4.8
	D-adaptive	5	5	4.9	4.8	4.8	4.8
D	MOSPA|$\mathcal{Q}$	92	171	253	420	634	1061
	C-adaptive	15.2	17.7	18.1	18.4	18.3	18.2
	D-adaptive	16.7	19.4	20.1	20.5	20.4	20.3
E	MOSPA|$\mathcal{Q}$	102	167	434	589	718	1063
	C-adaptive	34.6	35.6	36.6	36.8	34.7	32.5
	D-adaptive	40	40.9	41.6	41.4	39.1	37.4
F	MOSPA|$\mathcal{Q}$	100	182	256	445	682	1090
	C-adaptive	58.1	56.9	56.8	57.2	58.1	57.6
	D-adaptive	64.2	62.2	62	62	62.3	61.2
G	MOSPA|$\mathcal{Q}$	91	193	285	404	543	1086
	C-adaptive	37.8	34	32.4	31.3	30.5	30.3
	D-adaptive	35.6	31.5	30	28.9	28.1	27.9

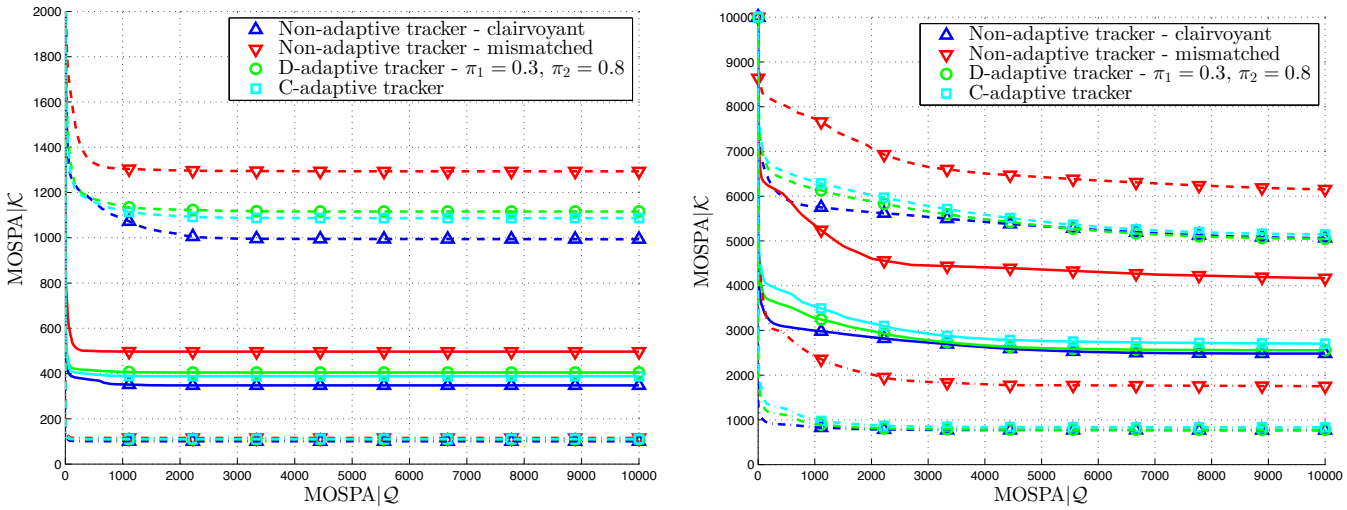

(a) True detection probability is 0.8 for all sensors.

(b) True detection probability is 0.3 for all sensors.

Fig. 3. MOSPA under $\mathcal{K}$ vs MOSPA under $\mathcal{Q}$ for the true detection probability fixed to 0.8 (a) and 0.3 (b) using one (dash lines), two (solid lines) and five sensors (dash-dot lines).

First, it is provided a comparison in terms of MOSPA for the scenario described in the previous subsection, see Fig. 2. As already observed the adaptive tracker exhibits better performance in the mid-interval (change of the detection probabilities from 0.9 to 0.3) because of its ability to react to the change of sensor performance with respect to the non-adaptive tracker, while there is not a great drawback in the other intervals when the two approaches seem equivalent. It is worthwhile to remark that when the target disappears at $k = 60$ the adaptive tracker has a spike in the error (observed also in the previous subsection) because of the delay in detecting the target disappearance. However, after few scans the error becomes equivalent to that of the non-adaptive tracker, which has a better capability to detect the target disappearance because uses a higher detection probability values.

Two other scenarios are analyzed in which the true detection probability is fixed at 0.8 (cf. Fig. 3(a)) and 0.3 (cf. Fig. 3(b)). In both cases, N varies in $\{1, 2, 5\}$ and the true detection probability is constant over all the time scans. Two non-adaptive trackers are considered: one *clairvoyant* that is correctly matched with the true value and another one that is mismatched (it uses 0.3 in Fig. 3(a) and 0.8 in Fig. 3(b)). Also, two adaptive trackers are considered: one continuous (C-adaptive tracker) and the other discrete (D-adaptive tracker). It is important to remark that while the D-adaptive requires lower computational effort with respect to C-adaptive, the C-adaptive requires fewer parameters, namely one: fixing the minimum level of the estimated distribution of the detection probability.

When varying the decision threshold p_γ compared with the posterior target presence, one obtains a pair of MOSPA values, under $\mathcal{Q}$ and $\mathcal{K}$ as in a receiver operating characteristic (ROC) curve [38]. The difference between curves in Fig. 3 and a ROC is that by using the MOSPA one achieves a compact evaluation of not only the tracker decision error, but also of the position error.

The MOSPA is evaluated averaging over 10^3 Monte Carlo runs and 20 time scans. All the sensors have a monostatic geometry. The target trajectory is generated in every Monte Carlo run with near constant velocity (cf. Section II). The D-adaptive tracker has two levels of detection probability, 0.3 and 0.8, matched with the true values of the examples and the transition matrix is

$$\boldsymbol{P}^s = \begin{bmatrix} 0.9 & 0.1 \\ 0.1 & 0.9 \end{bmatrix}.$$

The C-adaptive tracker has a minimum level $p^s_{min} = 0.2$ and $\sigma_s = 0.05$. The common parameters are specified in Tab. I.

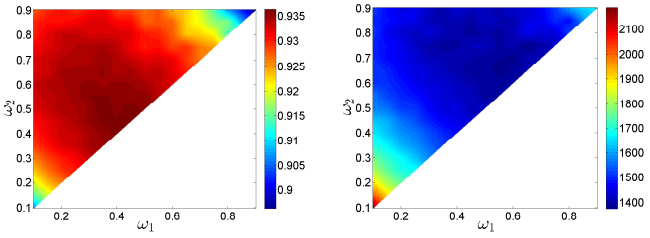

(a) Posterior target probability

(b) MOSPA

Fig. 4. Mean posterior target probability and MOSPA, scenario 1.

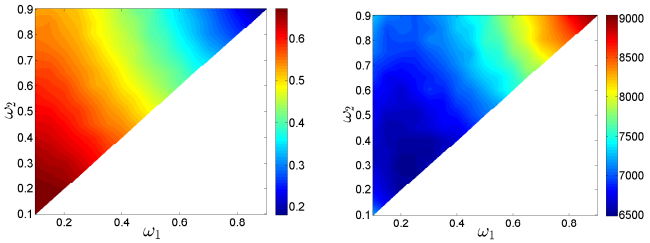

(a) Posterior target probability

(b) MOSPA

Fig. 5. Mean posterior target probability and MOSPA, scenario 2.

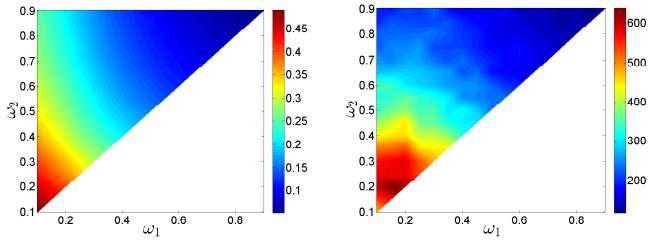

(a) Posterior target probability (b) MOSPA

Fig. 6. Mean posterior target probability and MOSPA, scenario 3.

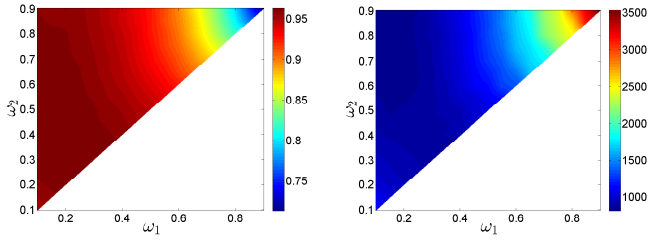

(a) Posterior target probability (b) MOSPA

Fig. 7. Mean posterior target probability and MOSPA, scenario 4.

It is shown in this scenario that both the adaptive trackers have performance close to the clairvoyant system exhibiting a gain in terms of MOSPA under $\mathcal{K}$ with respect to the mismatched non-adaptive tracker. Tab. II quantifies this gain for several values of MOSPA under $\mathcal{Q}$ in different scenarios. In particular, cases A, B and C refer to Fig. 3(a) for $N = 1, 2, 5$, respectively, while cases D, E and F refer to Fig. 3(b) for $N = 1, 2, 5$, respectively. In case G, a setup with five sensors has been used and the true detection probability is 0.8, the C-adaptive tracker uses $p^s_{min} = 0.2$, the D-adaptive tracker uses $\omega_1 = 0.2$, $\omega_2 = 0.8$, while the detection probability used in the non-adaptive tracker is 0.1.

The gain, reported in Tab. II, spans from a minimum of 4.8% to a maximum of 64%. The gain is substantial when the true detection probability is low (cf. Fig. 3(b)) while it becomes less significant in the other case (cf. Fig. 3(a)).

C. Sensitivity of the D-adaptive Tracker

This subsection presents an analysis of the sensitivity of the D-adaptive tracker when changing the values of the detection probabilities $\mathbf{\Omega} = \{\omega_1, \omega_2\}$. The case of a single monostatic sensor is considered with the same parameters as the previous subsection. The target probability and the MOSPA of the D-adaptive tracker are evaluated when assigning different values of ω_1 and ω_2, with $\omega_2 > \omega_1$. Both ω_1 and ω_2 are varied from 0.1 to 0.9 with a step equal to 0.05. It is worth noting that in the cases where $\omega_2 = \omega_1$, the D-adaptive tracker is equivalent to the non-adaptive tracker. Four setups are used in the simulations.

Scenario 1 (20 time scans):

- the target is always present;
- $p_k = 0.8$, $\forall k = 1, \ldots, 20$;

Scenario 2 (20 time scans):

- the target is always present;
- $p_k = 0.3$, $\forall k = 1, \ldots, 20$;

Scenario 3 (20 time scans):

- the target is always absent;
- the value of p_k is not relevant;

Scenario 4 (40 time scans):

- the target is always present;
- $p_k = \begin{cases} 0.8, & \forall k = 1, \ldots, 20, \\ 0.3, & \forall k = 21, \ldots, 40; \end{cases}$

The transition matrix of the D-adaptive tracker is the same as the previous subsection, while the target presence threshold is set to 0.8 for the scenarios 1, 2, 4 and to 0.6 for the scenario 3. The posterior target probability and the MOSPA are averaged over the time scans and Monte Carlo trials and the results for each scenario are shown in Figs. 4-7.

By inspection of Figs. 4-7, it is noted that there is a strong correlation between the MOSPA and the mean posterior target probability. Note that "good" here means a *high* (*low*) posterior target probability under $\mathcal{K}$ (under $\mathcal{Q}$) and *low* MOSPA. Furthermore, the MOSPA of a given scenario can be in contrast with the others. Specifically, scenario 1 and 3 are in agreement in the sense that the optimal setting of $\mathbf{\Omega}$ would be to select ω_1 and ω_2 both large. However, this is in contrast with scenario 2 and 4. As one might expect by intuition, scenarios 1 and 3 exhibit a large MOSPA when ω_1 and ω_2 are both small, while scenarios 2 and 4 exhibit a large MOSPA when ω_1 and ω_2 are both large. However, scenario 4 is to some extent equivalent to scenario 1 and 2 except for the transition at $k = 20$.

In Tab. III we compare the adaptive tracker, in which $\omega_1 = 0.3$ and $\omega_2 = .8$ are respectively small and large, with the non-adaptive tracker in which an intermediate value of the detection probability is used: namely $\omega_2 = \omega_1 = 0.5$. The implication is that the adaptive tracker is always better, but is especially so in last scenario in which there is the transition of the detection probability from a high value to a low value.

A good compromise is reached when ω_1 is small while ω_2 is large. This choice is in agreement with the adaptive tracking philosophy adopted in the previous subsections.

VI. Analysis using real-world data collected during CMRE sea trial experimentation

The results reported in this section are based on CMRE experimental campaigns where real-world data are collected. The first case of study is related to an HF-radar experiment, in

TABLE III
COMPARISON BETWEEN THE CASE $\omega_1 = \omega_2 = 0.5$ AND $\omega_1 = 0.3, \omega_2 = 0.8$

Scenario	ω_1	ω_2	MOSPA
1	0.5	0.5	1414
	0.3	0.8	1406
2	0.5	0.5	7140
	0.3	0.8	7054
3	0.5	0.5	238
	0.3	0.8	225
4	0.5	0.5	1110
	0.3	0.8	906

TABLE IV
PARAMETER VALUES USED IN THE ALGORITHM FOR REAL DATA.

Par.	*HFSW Radar*	*AUV*	*Specification*
T	33.28 s	48 s	Time scan
σ_v	$5\ 10^{-3}$ m/s^2	$5\ 10^{-2}$ m/s^2	Process noise
σ_r	75 m	100 m	Range standard deviation
σ_b	1°	1.5°	Bearing standard deviation
λ/V	$2\,10^{-9}$ m^{-2}	$3.1\,10^{-9}$ m^{-2}	Clutter density
N_p	$5\ 10^4$	$5\ 10^4$	Number of particles
p_b	10^{-4}	10^{-3}	Birth probability
p_s	$1-10^{-4}$	$1-10^{-5}$	Survival probability
N	2	2	Number of sensors
N_u	2500	2500	Uniform particles per scan
N_n	250	250	Particles per measurement
T_d	0.5	0.5	Degeneracy threshold
ν	10^4	10^4	Area of birth particles

which a network of HFSW radars was employed (see details in [28]). In this case we test only the C-adaptive tracker against the non-adaptive one, however similar results could be achieved using the D-adaptive.

The second case study is focused on the CMRE multistatic network of AUVs in the context of Anti-Submarine Warfare (ASW) (see details in [7], [11], [16]). The dataset was collected during ExPOMA12. In this case we test the D-adaptive tracker against the non-adaptive one.

A. Network of HFSW radars

Fig. 8 presents the results of the C-adaptive and non-adaptive trackers for a dataset collected during the CMRE HF-radar experiment [28]. Two Wellen radar (WERA) systems are considered. These systems are ultra-low power (around 50 W) HFSW radars developed mainly for ocean remote sensing applications, e.g., surface currents and sea state mapping, wind extraction, wave spectra analysis and, recently, tsunami early-warning detection.

WERA systems were deployed on the Italian coast of the Ligurian Sea, one on Palmaria island near La Spezia (44° $2'$ $30''$ N, 9° $50'$ $36''$ E) and the other at San Rossore Park near Pisa (43° $40'$ $53''$ N, 10° $16'$ $52''$ E). The target state is defined in Cartesian coordinates, with a fixed origin located at the Palmaria radar site.

Consider the real track of the vessel shown in Fig. 9 sailing North-West, as reported by the data transmitted by its Automatic Identification System (AIS) transponder. The AIS track positions, based on GPS, are referred to here as the ground-truth (see also the discussion in [28]). Fig. 8(a) reports the history of contacts of both the radars, the true target trajectory and the tracks generated by the C-adaptive tracker and the non-adaptive one. Fig. 8(b) is a zoom-in of Fig. 8(a) showing only the tracks.

The parameters of the algorithms are reported in the second column of Tab. IV. Note that all of the parameters for each of the algorithms are identical, including the number of particles, even though state augmentation should require, in theory, a larger number of particles. Furthermore, the C-adaptive tracker uses $p^s_{min} = 0.1$ and $\sigma_s = 0.05$ for both radars.

From the results reported in Fig. 8(b) it is easy to verify that the target trajectory is completely reconstructed by the C-adaptive tracker while the non-adaptive tracker exhibits some "gaps" in the estimated track. This phenomenon seems to be caused by abrupt decreases of the detection probability in one (or both) of the two radars with respect to the nominal values, which were calibrated and fixed to 0.9 for the non-adaptive tracker. Calibrating the values for a non-adaptive tracker is often an ad-hoc process [28]. The C-adaptive tracker has the ability to follow these apparent oscillations in detection probability (see Fig. 8(c)), resulting in much better track hold.

Figs. 8(d) and 8(e) report the estimation error in position and speed, respectively, assuming that the target is always declared as present. It can be noticed that the C-adaptive tracker outperforms the non-adaptive one in terms of error. In particular, as observed in the previous simulation, cf. Fig. 1, when the non-adaptive tracker has a small posterior target presence probability, it exhibits an error that can be an order of magnitude larger than the C-adaptive tracker.

B. Network of multistatic AUVs

The results reported in this section are based on the CMRE experimental campaign using the real-world data collected during ExPOMA12 in which the CMRE multistatic network of AUVs is tested. In [7], [11], [16] the problem of the port-starboard ambiguity is studied assuming that the target is always present. In [5], the cognitive paradigm is exploited in which the AUVs adaptively adjust their path in order to optimize the target detection capabilities.

ExPOMA12 was held in the Mediterranean Sea (Sicily, Italy) during February-March 2012. The target is represented by an echo-repeater (ER) that is towed by the NATO research vessel (NRV) *Alliance*. The main tool of research for the sea trials was CMRE's Ocean Explorer (OEX) AUV used in combination with the BENS towed-array. The OEX is an untethered AUV of length 4.5 m and diameter of 0.53 m. It can operate to a depth of 300 m and it has a maximum speed through the water of 3 knots, when towing the array. Battery constraints limit the lifetime of any mission to about 7 hours. The OEX is equipped with two independent WHOI modems for communication of data with the command centre and for passing of information between vehicles.

The BENS array is an adaption of the Slim Towed Array for AUV applications (SLITA) [24] and as such is based on the same underlying technology. The array has 83 hydrophones of which sets of 32 can be chosen for beamforming and processing. Furthermore, the array is equipped with 3 compasses and two depth sensors to aid with the reconstruction of the dynamics of the array.

The Deployable Experimental Multistatic Undersea Surveillance (DEMUS) source is a programmable bottom-tethered source capable of high source levels based on free-flooded ring technology. It is equipped with a WHOI modem which allows it to be turned on and off remotely by means of another compliant acoustic modem. The DEMUS source is equipped with a radio buoy so that the acoustic signals to be transmitted can be controlled by means of a radio connection.

In this scenario we compare the D-adaptive and the non-adaptive trackers, see Fig. 10. The setup of the experiment is given in Fig. 10(a), where we depict the location of the

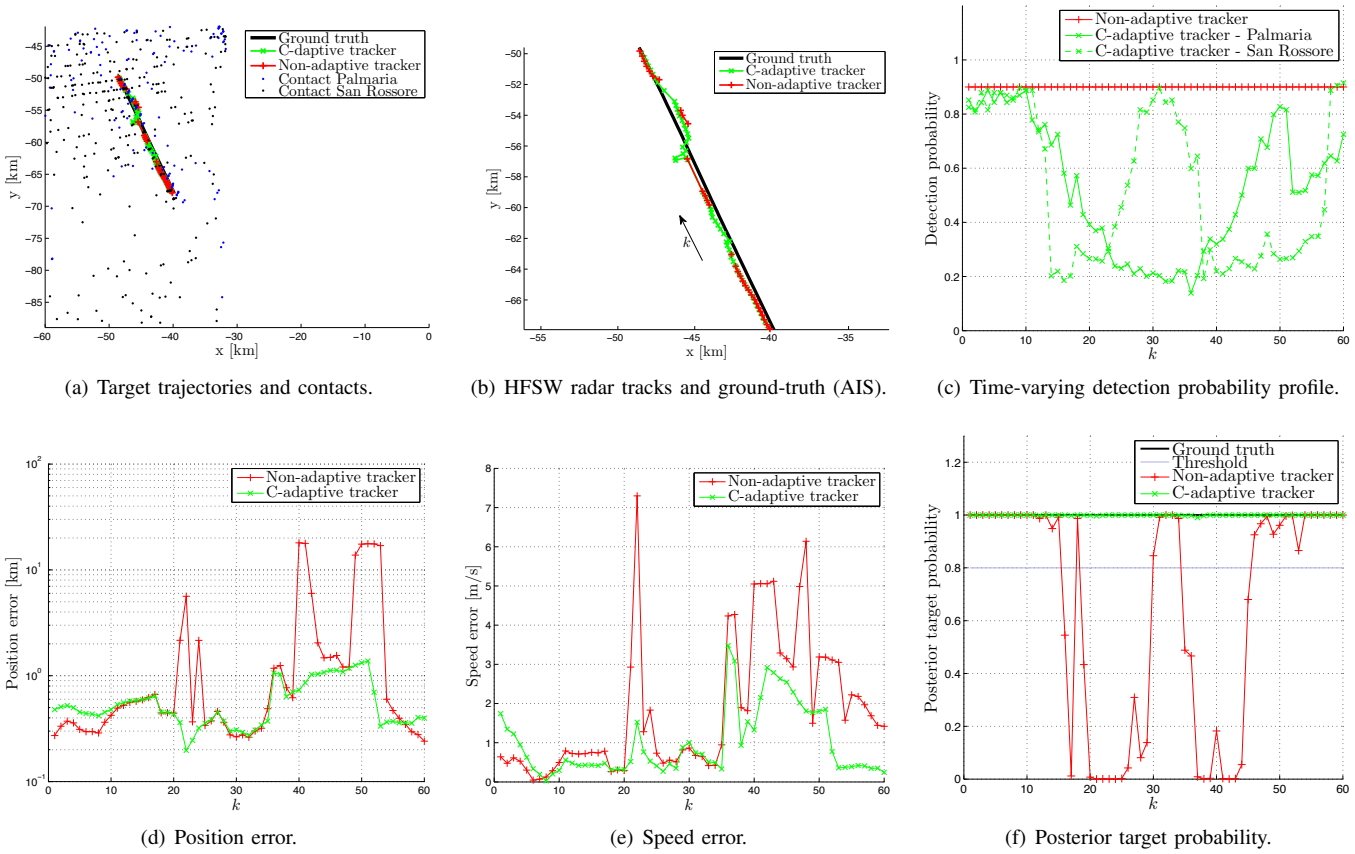

(a) Target trajectories and contacts.

(b) HFSW radar tracks and ground-truth (AIS).

(c) Time-varying detection probability profile.

(d) Position error.

(e) Speed error.

(f) Posterior target probability.

Fig. 8. Comparison between the C-adaptive and non-adaptive tracker using the dataset of two HFSW radar systems (WERA). Panel (a) shows the surveillance area with the target trajectories and the contacts. Panel (b) presents the trajectories when the target is declared as present and the ground-truth given by the AIS messages. Panel (c) presents the value of the detection probability, constant and fixed to 0.9 for the non-adaptive tracker, while for the C-adaptive tracker the mode of the posterior distribution of the detection probability for the two sensors, Palmaria and San Rossore, is shown. Panels (d) and (e) report the error between the estimated track the ground-truth in position and speed, respectively. Panel (f) presents the posterior target probability.

Fig. 9. A picture of the ship Höegh London tracked in the HFSW radar experiment.

DEMUS (diamond), the trajectories of the AUVs (Harpo in blue and Groucho in black), and of the ER (black thick line). The source is located at $(12.3\,\text{km}, 23.2\,\text{km})$. The target sails from the location $(16.5\,\text{km}, 16.9\,\text{km})$ to $(17.2\,\text{km}, 9.8\,\text{km})$ and then goes to $(11.3\,\text{km}, 15.8\,\text{km})$. The AUVs sail south-east of the source position and the target trajectory. For both sensors the D-adaptive tracker has two levels of detection probability, 0.2 and 0.8, and expected sojourn time in each state of 10 samples, while the non-adaptive tracker uses the value 0.8. The common parameter values for ExPOMA12 are reported in the third column of Tab. IV.

Fig. 10(b) reports the history of contacts of both the AUVs, the true target trajectory and the tracks generated by the D-adaptive tracker and the non-adaptive one. Fig. 10(c) is a zoom-in of Fig. 10(b) showing only the tracks. As already observed in the case of HFSW radar network, the adaptive tracker has the capability to completely reconstruct the target trajectory while the non-adaptive tracker fails to maintain hold of the target track. Moreover, the non-adaptive tracker exhibits some false alarms in the west region with respect to the target trajectory. Interestingly, the target track is lost by the non-adaptive tracker during the sharp maneuver around the location $(17.2\,\text{km}, 9.8\,\text{km})$ while it is held by the D-adaptive tracker.

Fig. 10(d) reports the estimation error in position, assuming that the target is always declared as present. The D-adaptive and non-adaptive trackers have similar performance when the target is declared as present. However, as already observed in the simulations (cf. Fig. 1) and in the case of the radar (cf. Fig. 8(d)) when the non-adaptive tracker loses the target ($20 < k < 40$ and $60 < k < 80$), it exhibits an error that can

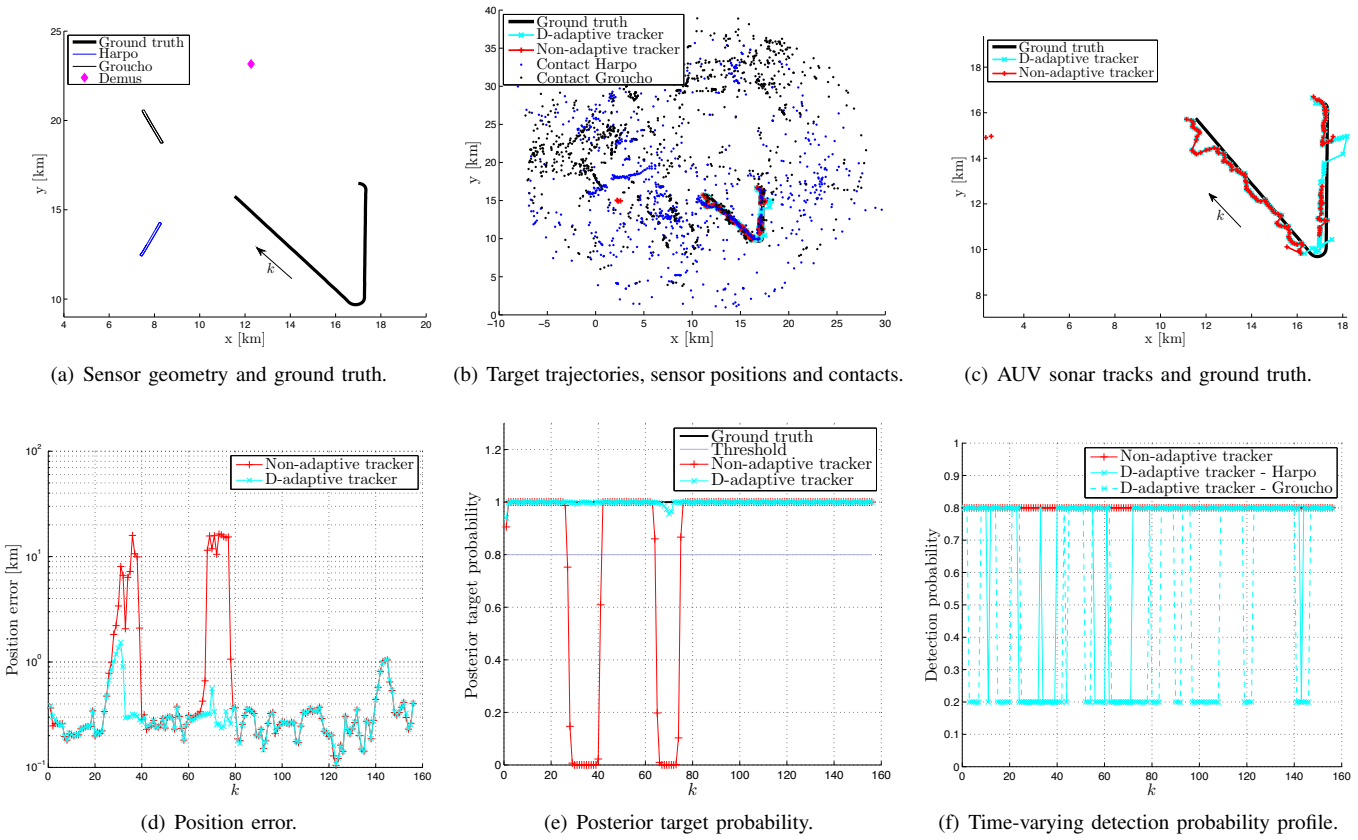

(a) Sensor geometry and ground truth.

(b) Target trajectories, sensor positions and contacts.

(c) AUV sonar tracks and ground truth.

(d) Position error.

(e) Posterior target probability.

(f) Time-varying detection probability profile.

Fig. 10. Comparison between the D-adaptive and non-adaptive tracker using the dataset of two AUV sonar array systems. Panel (a) depicts the setup of the experiment with the true target track, the trajectories of the receivers Harpo and Groucho and the position of the source Demus. Panel (b) shows the surveillance area with the target trajectories and the contacts. Panel (c) presents the trajectories, when the target is declared as present, and the ground-truth. Panel (d) presents the error between the estimated target position and the ground-truth. Panel (e) presents the posterior target probability. Panel (f) presents the value of the detection probability, constant and fixed to 0.8 for the non-adaptive tracker, while for the D-adaptive tracker the mode of the posterior distribution of the detection probability for the two sensors, Harpo and Groucho, is shown.

be an order of magnitude larger than the D-adaptive tracker.

VII. Conclusions

This paper presented a target tracking procedure, developed for a network of sensors, that is able to adapt and react to the time-varying changes of the sensors' target detection probability. The proposed tracking strategy is based on a Bayesian framework, and the implementation of the tracker is based on the particle filtering approach for RFS. The dynamic target state is augmented to include the sensors' detection probabilities.

The method was validated using computer simulations and real-world experiments, conducted by the NATO Science and Technology Organization (STO) - Centre for Maritime Research and Experimentation (CMRE). The improvements with respect to the non-adaptive tracker are demonstrated in terms of the MOSPA metric reaching approximately the performance of the clairvoyant system which knows the true sensor network detection probabilities.

A great improvement over the non-adaptive tracking approach is demonstrated using real-world data from both a network of HFSW radars and a multistatic network of AUVs.

Future investigations include the generalization of the proposed method to the case of several sensors and several targets, based on the belief propagation (BP). The BP approach leads to an innovative solution of the general Bayesian formulation of multi-target multi-sensor tracking problems [30], [31] in which it is possible to include the probabilistic "time-varying" feature of the detection probability formalized in the proposed work.

Besides the adopted multi-target strategy, a high track density may lead to poor performance of the tracker because of the complexity of the problem itself in which not only it is requested to track a *large* and *unknown* number of targets but also their associated detection probabilities.

Acknowledgment

This work has been funded by the NATO Allied Command Transformation (NATO-ACT) under the project Maritime Situational Awareness.

References

[1] M. Arulampalam, S. Maskell, N. Gordon, and T. Clapp, "A tutorial on particle filters for online nonlinear/non-Gaussian Bayesian tracking," *IEEE Trans. Signal Process.*, vol. 50, no. 2, pp. 174 –188, Feb. 2002.

[2] Y. Bar-Shalom, P. Willett, and X. Tian, *Tracking and Data Fusion: A Handbook of Algorithms*. Storrs, CT: YBS Publishing, 2011.

[3] M. Basseville and I. V. Nikiforov, *Detection of Abrupt Changes: Theory and Application*. Englewood Cliffs, N.J: Prentice-Hall, 1993.

[4] W. Blanding, P. Willett, Y. Bar-Shalom, and S. Coraluppi, "Multisensor track management for targets with fluctuating SNR," *IEEE Trans. Aerosp. Electron. Syst.*, vol. 45, no. 4, pp. 1275–1292, Oct 2009.

[5] P. Braca, R. Goldhahn, K. LePage, P. Willett, S. Marano, and V. Matta, "Cognitive multistatic auv networks," in *Proc. of the* 17^{th} *Intern. Conf. on Inform. Fusion (FUSION)*, Salamanca, 2014.

[6] P. Braca, M. Guerriero, S. Marano, V. Matta, and P. Willett, "Selective measurement transmission in distributed estimation with data association," *IEEE Trans. Signal Process.*, vol. 58, no. 8, pp. 4311–4321, Aug. 2010.

[7] P. Braca, K. LePage, P. Willett, S. Marano, and V. Matta, "Particle filtering approach to multistatic underwater sensor networks with left-right ambiguity," in *Proc. of the* 16^{th} *Intern. Conf. on Inform. Fusion (FUSION)*, Istanbul, 2013.

[8] P. Braca, S. Marano, V. Matta, and P. Willett, "Multitarget-multisensor ML and PHD: Some asymptotics," in *Proc. of the* 15^{th} *Intern. Conf. on Inform. Fusion (FUSION)*, Singapore, 2012.

[9] ——, "Asymptotic efficiency of the PHD in multitarget/multisensor estimation," *IEEE J. Sel. Topics Signal Process.*, vol. 7, no. 3, pp. 553–564, 2013.

[10] ——, "A linear complexity particle approach to the exact multi-sensor PHD," in *in Proc. IEEE Int. Conf. Acoust., Speech, Signal Process. (ICASSP)*, May 2013.

[11] P. Braca, P. Willett, K. LePage, S. Marano, and V. Matta, "Bayesian tracking in underwater wireless sensor networks with port-starboard ambiguity," *IEEE Trans. Signal Process.*, vol. 62, no. 7, pp. 1864–1878, Apr. 2014.

[12] S. Challa, B.-N. Vo, and X. Wang, "Bayesian approaches to track existence - IPDA and random sets," in *Proc. of the Fifth International Conference on Information Fusion*, vol. 2, July 2002, pp. 1228–1235 vol.2.

[13] D. Clark, B. Ristic, B.-N. Vo, and B.-T. Vo, "Bayesian multi-object filtering with amplitude feature likelihood for unknown object SNR," *IEEE Trans. Signal Process.*, vol. 58, no. 1, Jan 2010.

[14] S. Coraluppi and D. Grimmett, "Multistatic sonar tracking," in *Proc. of SPIE Conference on Signal Processing, Sensor Fusion, and Target Recognition XII*, Orlando FL, USA, Apr. 2003.

[15] O. Erdinc, P. Willett, and Y. Bar-Shalom, "The bin-occupancy filter and its connection to the PHD filters," *IEEE Trans. Signal Process.*, vol. 57, no. 11, pp. 4232–4246, Nov. 2009.

[16] R. Goldhahn, P. Braca, K. LePage, P. Willett, S. Marano, and V. Matta, "Environmentally sensitive particle filter tracking in multistatic AUV networks with port-starboard ambiguity," in *Proc. IEEE Int. Conf. Acoust., Speech, Signal Process. (ICASSP)*, Florence, 2014.

[17] I. R. Goodman, R. P. Mahler, and H. T. Nguyen, *Mathematics of data fusion*. Dordrecht, The Netherlands: Kluwer Academic Publisher, 1997.

[18] E. Hanusa and D. Krout, "Track state augmentation for estimation of probability of detection in multistatic sonar data," in *Proc. of the Asilomar Conference on Signals, Systems and Computers*, Nov 2013, pp. 1733–1737.

[19] S. Horn, "Near real time estimation of surveillance gaps," in *Proc. of the* 16^{th} *Intern. Conf. on Inform. Fusion (FUSION)*, July 2013, pp. 1871–1877.

[20] K. Jamieson, M. Gupta, and D. Krout, "Sequential bayesian estimation of the probability of detection for tracking," in *Proc. of the* 12^{th} *International Conference on Information Fusion*, July 2009, pp. 641–648.

[21] H. Kennedy, "Powerful test statistic for track management in clutter," *IEEE Trans. Aerosp. Electron. Syst.*, vol. 50, no. 1, pp. 207–223, January 2014.

[22] T. Kirubarajan, Y. Barshalom, K. Pattipati, and I. Kadar, "Ground target tracking with variable structure IMM estimator," *IEEE Trans. Aerosp. Electron. Syst.*, vol. 36, no. 1, pp. 26–46, Jan. 2000.

[23] C. Kreucher, A. Hero, and K. Kastella, "A comparison of task driven and information driven sensor management for target tracking," in *44th IEEE Conf. on Decision and Control, 2005 and 2005 European Control Conference (CDC-ECC)*, 2005.

[24] A. Maguer, R. Dymond, M. Mazzi, S. Biagini, and S. Fioravanti, "SLITA: a new slim towed array for AUV applications," in *Acoustics'08*, 2008, pp. 141–146.

[25] R. Mahler, "Multitarget Bayes filtering via first-order multitarget moments," *IEEE Trans. Aerosp. Electron. Syst.*, vol. 39, no. 4, pp. 1152–1178, Jan. 2003.

[26] ——, *Statistical Multisource-Multitarget Information Fusion*. Artech House, 2007.

[27] R. Mahler, B.-T. Vo, and B.-N. Vo, "CPHD filtering with unknown clutter rate and detection profile," *Signal Processing, IEEE Transactions on*, vol. 59, no. 8, pp. 3497–3513, aug 2011.

[28] S. Maresca, P. Braca, J. Horstmann, and R. Grasso, "Maritime surveillance using multiple high-frequency surface-wave radars," *IEEE Trans. Geosci. Remote Sens.*, 2014.

[29] E. Mazor, A. Averbuch, , Y. Barshalom, and J. Dayan, "Interacting multiple model methods in target tracking: A survey," *IEEE Trans. Aerosp. Electron. Syst.*, vol. 34, no. 1, pp. 103–123, Jan. 1998.

[30] F. Meyer, P. Braca, P. Willett, and F. Hlawatsch, "Scalable multitarget tracking using multiple sensors: A belief propagation approach," in *Proc. of the* 18^{th} *International Conference on Information Fusion*, Washington D.C., USA, Jul. 2015, pp. 1778–1785.

[31] ——, "Tracking an unknown number of targets using multiple sensors: A belief propagation method," in *Proc. of the* 19^{th} *International Conference on Information Fusion*, 2016 (submitted).

[32] M. R. Morelande, C. M. Kreucher, and K. Kastella, "A Bayesian approach to multiple target detection and tracking," *IEEE Trans. Signal Process.*, vol. 55, no. 5, pp. 1589–1604, 2007.

[33] D. Musicki and R. Evans, "Joint integrated probabilistic data association: JIPDA," *IEEE Trans. Aerosp. Electron. Syst.*, vol. 40, no. 3, pp. 1093–1099, July 2004.

[34] D. Musicki, R. Evans, and S. Stankovic, "Integrated probabilistic data association," *IEEE Trans. Autom. Control*, vol. 39, no. 6, pp. 1237–1241, Jun 1994.

[35] R. Osborne, Y. Bar-Shalom, and T. Kirubarajan, "Radar measurement noise variance estimation with several targets of opportunity," *IEEE Trans. Aerosp. Electron. Syst.*, vol. 44, no. 3, pp. 985–995, July 2008.

[36] G. Papa, S. Horn, P. Braca, K. Bryan, and G. Romano, "Estimating sensor performance and target population size with multiple sensors," in *Proc. of the* 15^{th} *Intern. Conf. on Inform. Fusion (FUSION)*, jul 2012, pp. 2102–2109.

[37] G. Papa, P. Braca, S. Horn, S. Marano, V. Matta, and P. Willett, "Adaptive bayesian tracking with unknown time-varying sensor network performance," *submitted to 40th IEEE Int. Conf. on Acoust., Speech and Signal Process. (ICASSP)*, 2015.

[38] H. V. Poor, *An Introduction to Signal Detection and Estimation*. New York: Springer-Verlag, 1988.

[39] B. Ristic, D. Clark, B.-N. Vo, and B.-T. Vo, "Adaptive target birth intensity for PHD and CPHD filters," *IEEE Trans. Aerosp. Electron. Syst.*, vol. 48, no. 2, pp. 1656–1668, apr 2012.

[40] B. Ristic, B.-T. Vo, B.-N. Vo, and A. Farina, "A tutorial on Bernoulli filters: Theory, implementation and applications," *IEEE Trans. Signal Process.*, vol. 61, no. 13, pp. 3406–3430, July 2013.

[41] D. Schuhmacher, B.-T. Vo, and B.-N. Vo, "A consistent metric for performance evaluation of multi-object filters," *IEEE Trans. Signal Process.*, vol. 56, no. 8, pp. 3447–3457, Aug. 2008.

[42] L. Svensson, D. Svensson, M. Guerriero, and P. Willett, "Set JPDA filter for multitarget tracking," *IEEE Trans. Signal Process.*, vol. 59, no. 10, pp. 4677–4691, Oct. 2011.

[43] B.-N. Vo, S. Singh, and A. Doucet, "Sequential Monte Carlo methods for multitarget filtering with random finite sets," *IEEE Trans. Aerosp. Electron. Syst.*, vol. 21, no. 4, pp. 1224–1245, 2005.

[44] B.-T. Vo, B.-N. Vo, and A. Cantoni, "Bayesian filtering with random finite set observations," *IEEE Trans. Signal Process.*, vol. 56, no. 4, pp. 1313–1326, Apr. 2008.

[45] B.-T. Vo, B.-N. Vo, R. Hoseinnezhad, and R. Mahler, "Robust multi-bernoulli filtering," *IEEE J. Sel. Topics Signal Process.*, vol. 7, no. 3, pp. 399–409, June 2013.

[46] H. Wang, T. Kirubarajan, and Y. Bar-Shalom, "Precision large scale air traffic surveillance using IMM/assignment estimators," *IEEE Trans. Aerosp. Electron. Syst.*, vol. 35, no. 1, pp. 255–266, Jan. 1999.